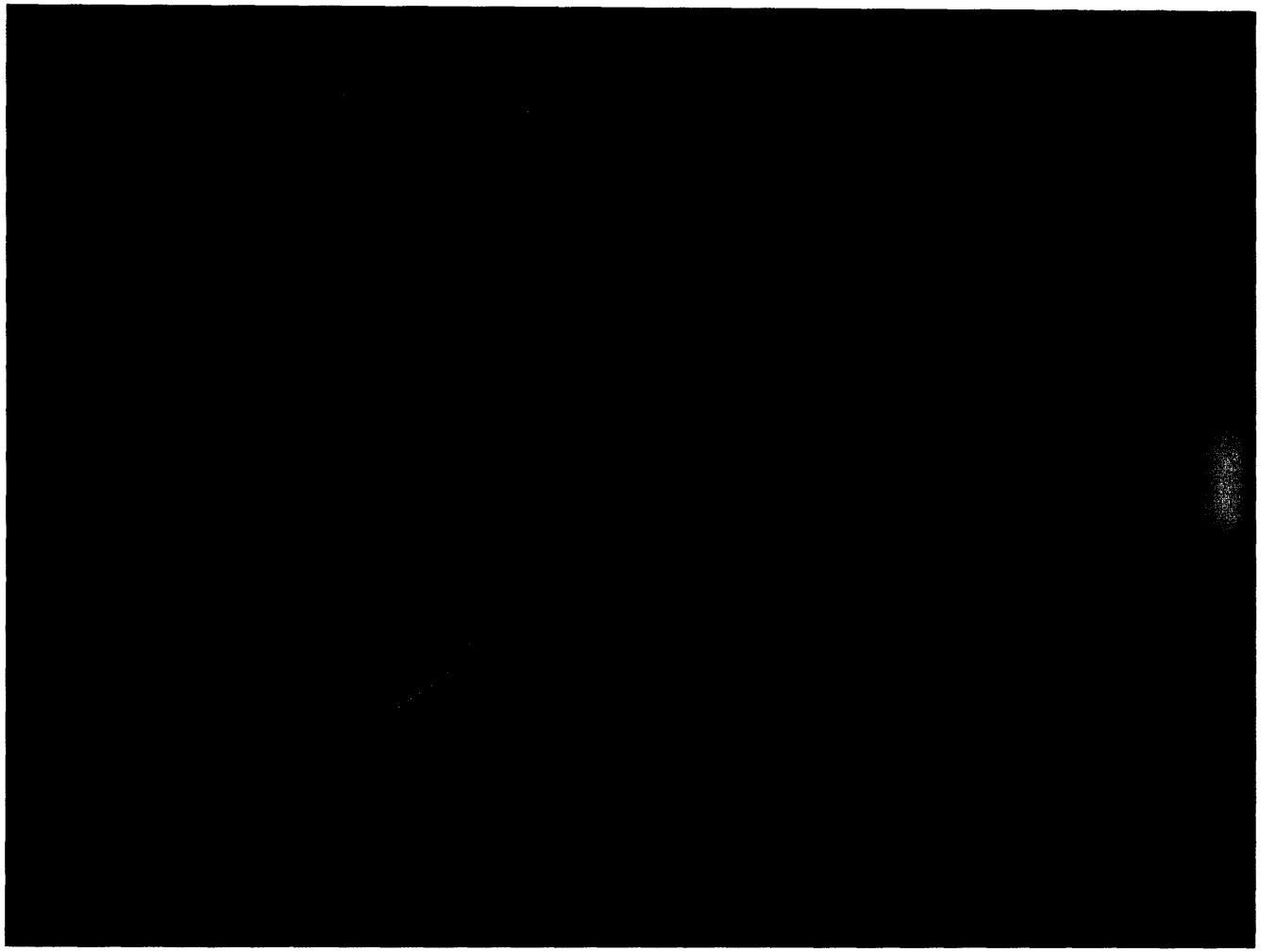

**Fig. 4.13. Concluded.**
**(c) As Surface Contours in USAERO**

# APPENDIX E

Calculations by YNU

# Calculation by Surface Vortex Lattice Method

H.Yamasaki Yokohama National University, Japan

Aug. 23, 1992

## 1 Numerical Computing Procedure of Surface Vortex Lattice Method

When a propeller rotates in steady condition, there are generated spanwise and chordwise vortices on the real blade surface and trailing vortices in wake.
By applying Kerwin's formula(1) based on the principle of conservation of circulation, we can replace chordwise vortex and trailing vortex in terms with only discrete spanwise vortices.
In the vortex lattice method, the lifting surface on the mean camber surface of each blade is represented by horse-shoe vortices and the effects of thickness are done by sources. The strength of sources is determined by thin thickness assumption.
Now, in the surface vortex lattice method, the vortex lattice is placed just on the blade surface, and these vortices on the body surface play a part of not only the effect of camber but thickness. Consequently, only the strengths of spanwise vortices on the surface are unkown variables.
A blade surface is divided into several discrete elements, each of which is represented by a horse-shoe vortex.
Analytical expressions are derived for the perturbation velocity field induced by each horse- shoe vortex (vortex lattice). These are deduced to calculate the coefficients of a system of linear equations relating the magnitude of the normal velocity at each control point on the blade surface to the unknown spanwise vortex strength. So as to satisfy the boundary condition at the control points the spanwise vortex strengths are determined by solving this system of equations by an iterative procedure.
The boundary condition is given by the equation

$$\boldsymbol{V}_i \cdot \boldsymbol{n}_i = 0 \tag{1}$$

,where $\boldsymbol{V}_i$ is the resultant velocity vector and $\boldsymbol{n}_i$ is the normal vector to the blade surface at the i-th control point. The resultant velocity $\boldsymbol{V}_i$ at the i-th control point is summation of induced velocities by the vortex lattices, and undisturbed inflow velocity.
Specifically,

$$\boldsymbol{V}_i = \boldsymbol{V}_{iG} + \boldsymbol{V}_{iu} \tag{2}$$

,where $\boldsymbol{V}_{iG}$ is the velocity induced by the votrices relating the propeller, $\boldsymbol{V}_{iu}$ is the undisturbed inflow at i-th control point.

Considering this fact and equation (2), equation (1) becomes the following equation.

$$\boldsymbol{V}_{iG}\cdot\boldsymbol{n}_i = -\boldsymbol{n}_i\cdot\boldsymbol{V}_{iu} \tag{3}$$

We can transform equation (3) with respect to the strengths of spanwise vortices as unknown variables.

$$\sum_{k=1}^{K}\left[\sum_{m=1}^{M}\sum_{n=1}^{N}\Gamma_{nm}^{B}\cdot\left\{u_{inm}^{B\square}(k)+\sum_{n_w=2}^{N_w}u_{inm}^{Bw}(k)\right\}\right.$$
$$\left.+\sum_{m=1}^{M}\sum_{n=1}^{N}\Gamma_{nm}^{F}\cdot\left\{u_{inm}^{F\square}(k)+\sum_{n_w=2}^{N_w}u_{inm}^{Fw}(k)\right\}\right]=d_i \tag{4}$$

,where

$$d_i = -\boldsymbol{n}_i\cdot\boldsymbol{V}_{iu} \tag{5}$$

| | | |
|---|---|---|
| $K$ | : | number of propeller blades |
| $M$ | : | number of spanwise vortex elements of a propeller blade |
| $N$ | : | number of chordwise vortex elements of a propeller blade |
| $N_w$ | : | number of trailing vortex elements of propeller wake |
| $\Gamma_{nm}$ | : | strength of spanwise vortex at n-th chordwise and m-th spanwise |
| $u_i^{\square}$ | : | normal component of the velocity at the i-th control point induced by unit ring vortex on propeller blade |
| $u_i^{w}$ | : | normal component of the velocity at the i-th control point induced by unit trailing vortex in propeller wake |
| $B, F$ | : | index of back side or face side of blade |

The $u_{inm}^{B\square}$ in the equation (4) means normal induced velocity at the i-th control point by a ring vortex at n-th chordwise and m-th spanwise on the back side surface having unit strength.
The velocity induced by a ring vortex can be calculated by Biot - Savart law.
The continuous vortex distribution representing the blade element is replaced with discrete one, which is placed at the front edge of the small panel and the control point is taken at the point of half chord as shown Fig.1 .
The two vortices on the back and face surfaces which are the closest to the leading edge are placed at a distance of $\alpha \cdot C$. The $C$ is a chord length and $\alpha$ is 0.01 in this calculation.
We obtained the fact that the singularity between vortices near the sharp trailing edge as propeller blade is too strong to get good accuracy solutions.
In the present method, to avoid this the real surface panels satisfying the following expression are replaced by lifting surface panels.

$$\frac{b}{a} < \beta \tag{6}$$

The a means distance from spanwise vortex to control point on the back side and the b is distance from spanwise vortex on the opposite face side to control point on the back side, the $\beta$ is a constant value and it is taken 1.025.

# 2 Division of Propeller Blade and Wake Model

## 2.1 Propeller Blade

The back and face surface of a propeller blade are divided into $N \times M$ panels.
In the chordwise spacing, same spacing is selected and in the spanwise spacing, cosine spacing used by Hoshino(2) is adopted.

$$r_m = \frac{1}{2}(r_t + r_h) - \frac{1}{2}(r_t - r_h)cos\alpha_m \tag{7}$$

$$\alpha_m = \begin{cases} 0 & for \quad m = 1 \\ \frac{(2m-1)\pi}{2(M+1)} & for \quad m = 2, 3, \ldots, M+1 \end{cases} \tag{8}$$

,where $r_m$ are radial positions of the corner points of each panels and $r_h$ is the radius of the boss, the $r_t$ are radial distances represented by following expression.

$$r_t = \frac{(r - r_h)(4M+1)}{4M+2} \tag{9}$$

## 2.2 Propeller Wake Model

Fig.2 shows that the geometry of the propeller wake was simulated by iterative procedure. In the first step, we calculated the strengths of the vortices in the whole system including classical wake whose pitch distribution is equal to propeller's and which is not considered contraction and computed the induced velocity at each end of the segments of the discrete propeller wake, made them move to new position by using following expressions.

$$P_W^{(N+1)} = P_W^N + \boldsymbol{V}_W \cdot \Delta t \tag{10}$$

$$\boldsymbol{V}_W = (V_a + V_x, V_r, 2\pi nr + V_\theta) \tag{11}$$

,where $P_W^{(N)}$ are the coordinates of the ends of the discrete wake segments at N time step and each components of the $V_x, V_r, V_\theta$ are the axis, radial and circumferential induced velocity by vortex distribution respectively.
Moreover, the $\Delta t$ in the expression (10) is determined by the following expression

$$\Delta t = \frac{1}{n \cdot N_W} \tag{12}$$

,where the $n$ means the number of propeller revolution. After the second step, simulations are continued by the process as mentioned above untill thrust coefficients at each time step converge.

# 3 Calculation of Hydrodynamic Forces, Thrust and Torque

The hydrodynamic force acting on each discrete element has been composed of the following terms.

1. Kutta - Joukowski force acting on a ring vortex on the surface
2. Viscous drag at each blade element.

We can get the viscous drag working at each blade element by following equation

$$C_F = \left(1 + \frac{t_{max}}{C}\right) \cdot \frac{0.455}{(\log_{10} R_e)^{2.58}} \tag{13}$$

,where $t_{max}$ is maximum thickness of the each blade section and $R_e$ is the Reynolds number. The thrust and the torque of the propeller have been calculated by the summation of each components of the above terms.

# 4 Calculation of the Density of Circulation Distribution and the Pressure Distribution on the Blade

By applying Kerwin's formula, we have obtained the density of circulation distribution on i-th control point

$$\gamma_i = \frac{\Gamma^b_{nm} + \Gamma^b_{n+1,m}}{2\delta s} \tag{14}$$

,where $\gamma_i$ is the density of circulation distribution, $\Gamma^b_{nm}$ is the bound vortex at (n,m)-th panel, and $\delta s$ is the spanwise length of the panel.
According to Yuasa(3), the pressure at i-th control point has been calculated by using Bernoulli's equation.

$$C_{PB} = 1 - \frac{V_i^{B2}}{V_{iu}^2} \tag{15}$$

$$C_{PF} = 1 - \frac{V_i^{F2}}{V_{iu}^2} \tag{16}$$

$$V_i^B = \mid \boldsymbol{V}_i^B \mid + \left\{(\Gamma^{Bb}_{nm} + \Gamma^{Bb}_{n+1,m})/(4 \cdot \delta s)\right\} \tag{17}$$

$$V_i^F = \mid \boldsymbol{V}_i^F \mid - \left\{(\Gamma^{Fb}_{nm} + \Gamma^{Fb}_{n+1,m})/(4 \cdot \delta s)\right\} \tag{18}$$

# 5 Results and Discussions

In the present method, DTRC4119 propeller condition without hub and with devised wake as mentioned previously was selected.

### 5.1 Open Water Characteristics

Fig.3 shows comparison of experiments and calculations. The calculations were both with and without viscous.
The thrust coefficients of the calculations with viscous are in good agreements with the experimental results, but with respect to the torque coefficients, the lower advance coefficients are, the larger differences between them are. They were caused by lack of friction resistance which were calculated by the expression using in flat plate and no taking separation of the tip vortex into consideration.

### 5.2 Pressure Distribution

Fig.4,5,6 show pressure distribution on blade at 0.3, 0.7 and 0.9 radius respectively.
Fig.4 shows that the calculations are smaller than the experimental results on the whole chord, especialy the differences between them are remarkable at leading edge like other radial positions (Fig.5 and Fig.6). We suppose that the diffrences of estimations on the whole chord depend on the calculation condition without hub and the differences at leading edge were caused by great influence of the closest vortices to the leading edge and discontinuous panel arrangement.
Fig.5 shows that the calculations are in good agreements with the experimental results except for the neighborhood of the leading edge. The differences are caused by the reason as mentioned previously.
Fig.6 show that the calculations are not agree to the experimental results on the whole chord and they are unreal distribution. We think that the unreality of this distribution were induced by the singularity of the close vortices on opposite sides.

### 5.3 Pitch Distribution of Propeller Wake

Fig.7 shows pitch distribution of the propeller wake calculated by the iterative procedure. The distances from the center line are 0.328 and 0.95 radius.
Both of the calculation distributions are similar to the experimental results but they are not in good agreement. We think that the strengths of the innermost vortex and tip vortex are not calculated correctly.

## 6 References

1. Kerwin, J.E. and Lee, C. -S.:"Prediction of Steady and Unsteady Marine Propeller Performance by Numerical Lifting Surface Theory", Transactions of the Society of Naval Architects and Marine Engineers, Vol.86, 1978 pp.218-253

2. Hoshino, T.:Hydrodynamic Analysis of Propellers in Steady Flow Using a Sureface Panel Method, Journal of the Society of Naval Architects of Japan, Vol.165, 1989 pp.55-70

3. Yuasa, H.:"Application of Numerical Lifting-Surface Theory on Steady Performance of Propeller/Duct System", Journal of the Society of Naval Architects of Japan, Vol.147, 1980 pp.53-70

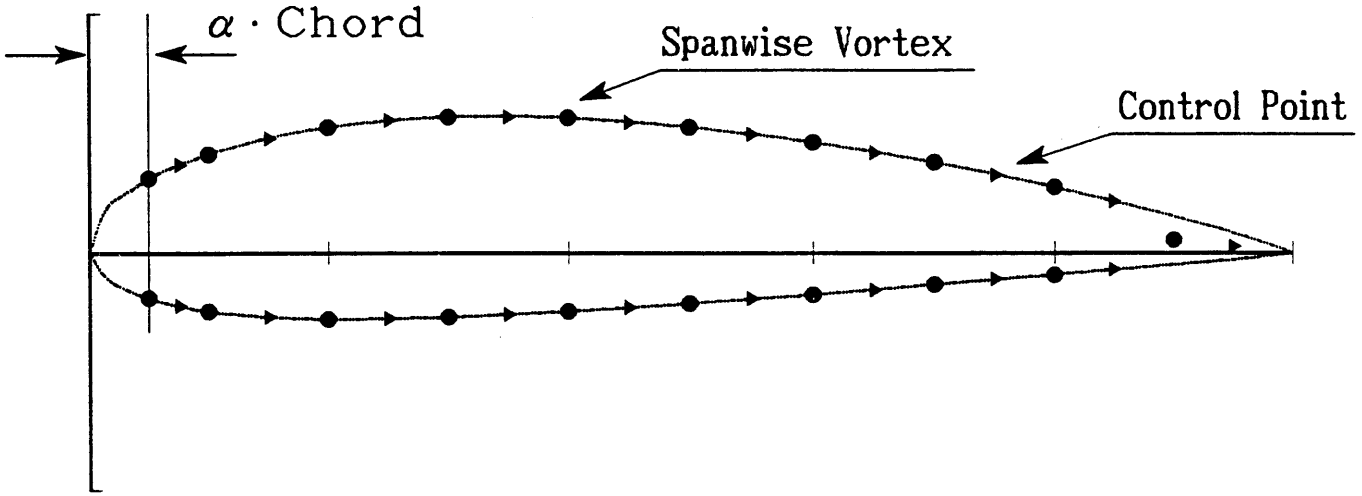


Fig. 1 Arrangement of Surface Vortex Lattice Model

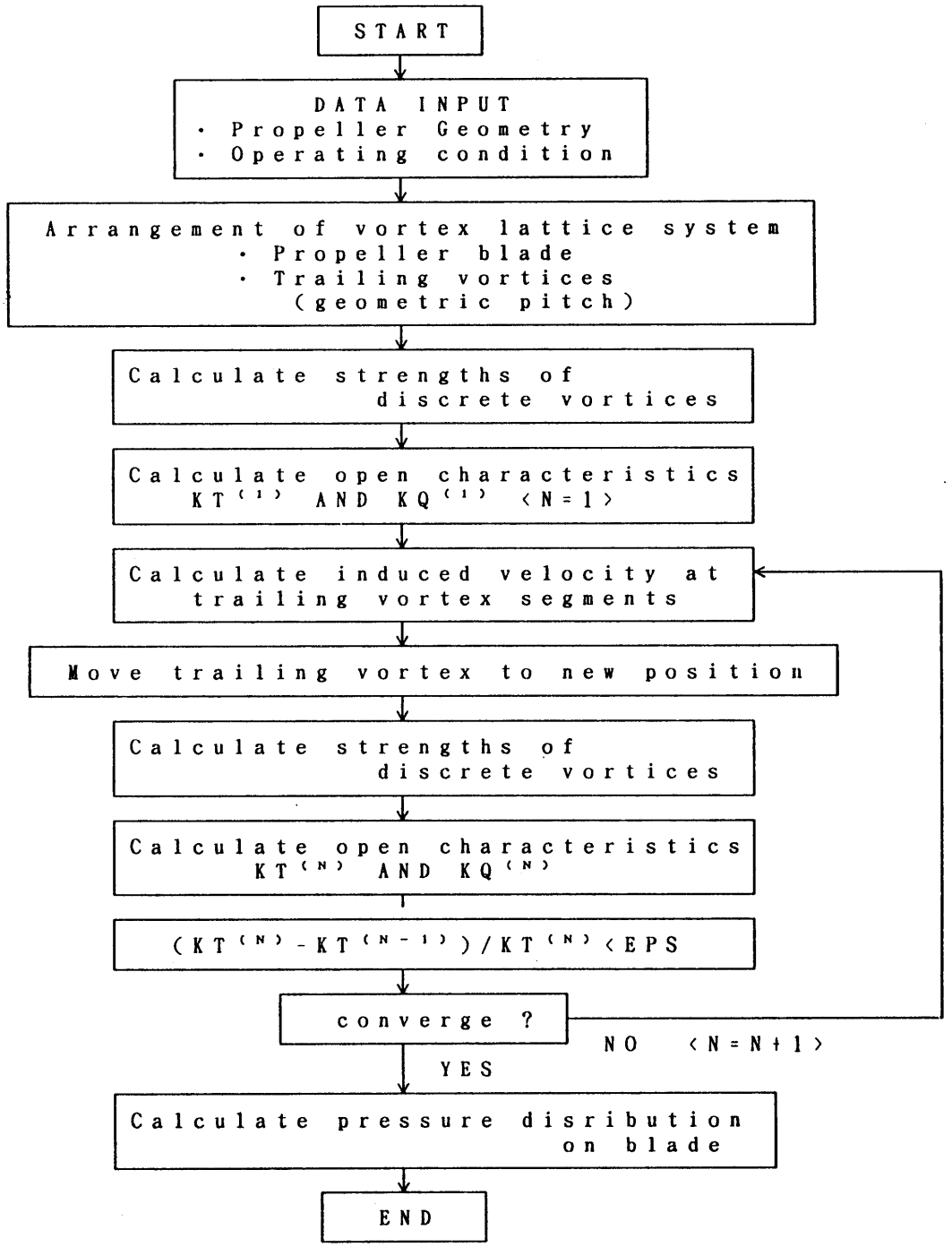


Fig. 2 Flow Chart of Present Calculation

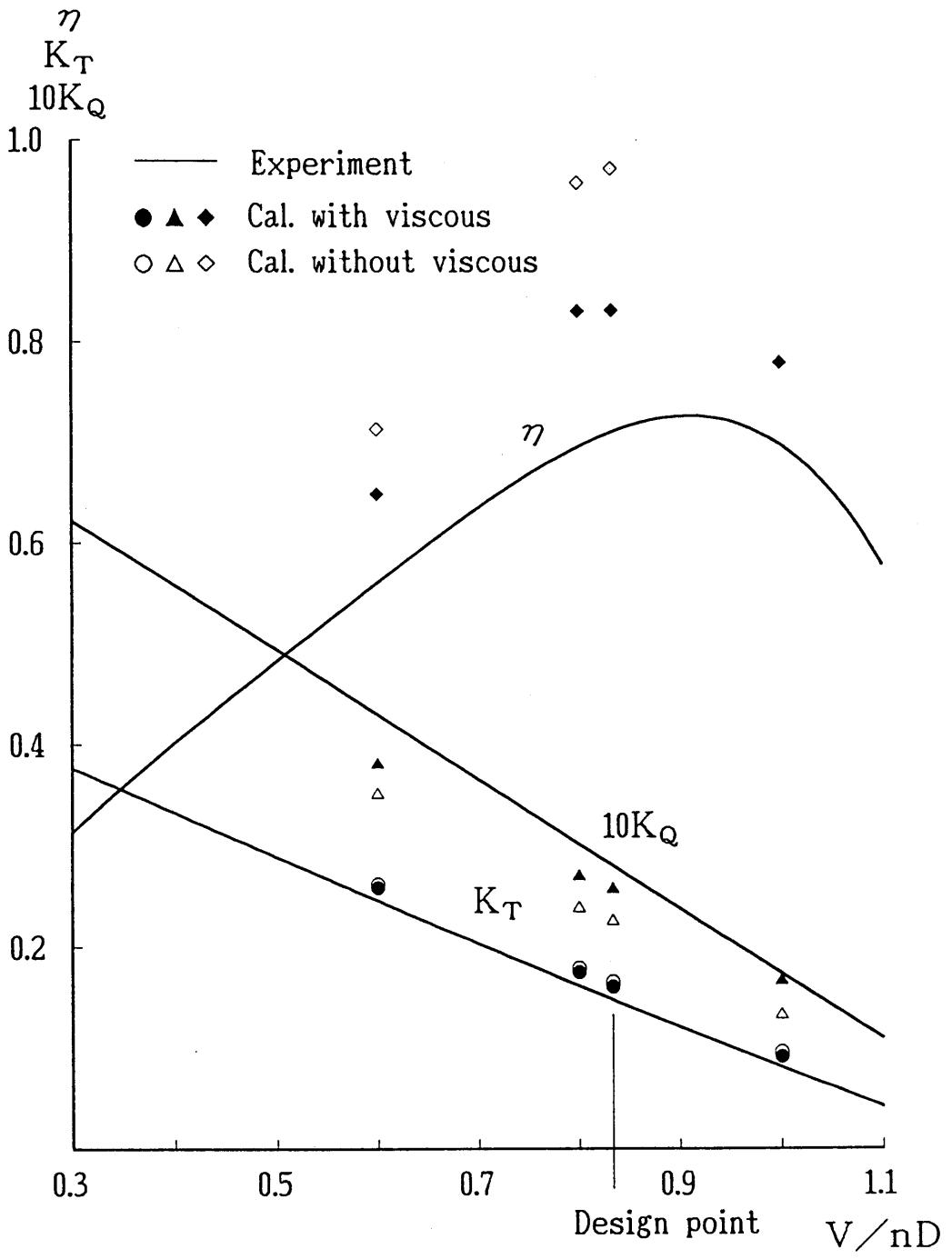


Fig. 3 Open Water Characteristics for Propeller(DTRC4119)
(Devised Wake)

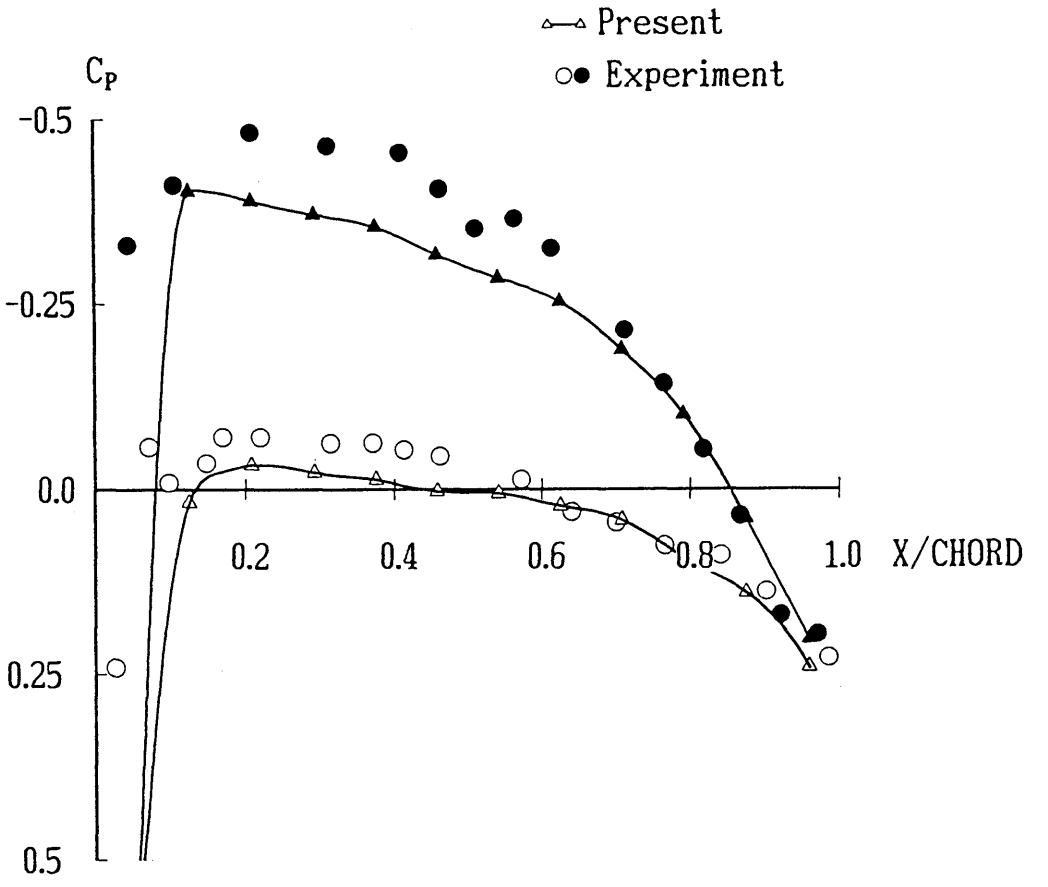


Fig. 4 Pressure distribution on DTRC4119
(Devised Wake, 0.3 Radius)

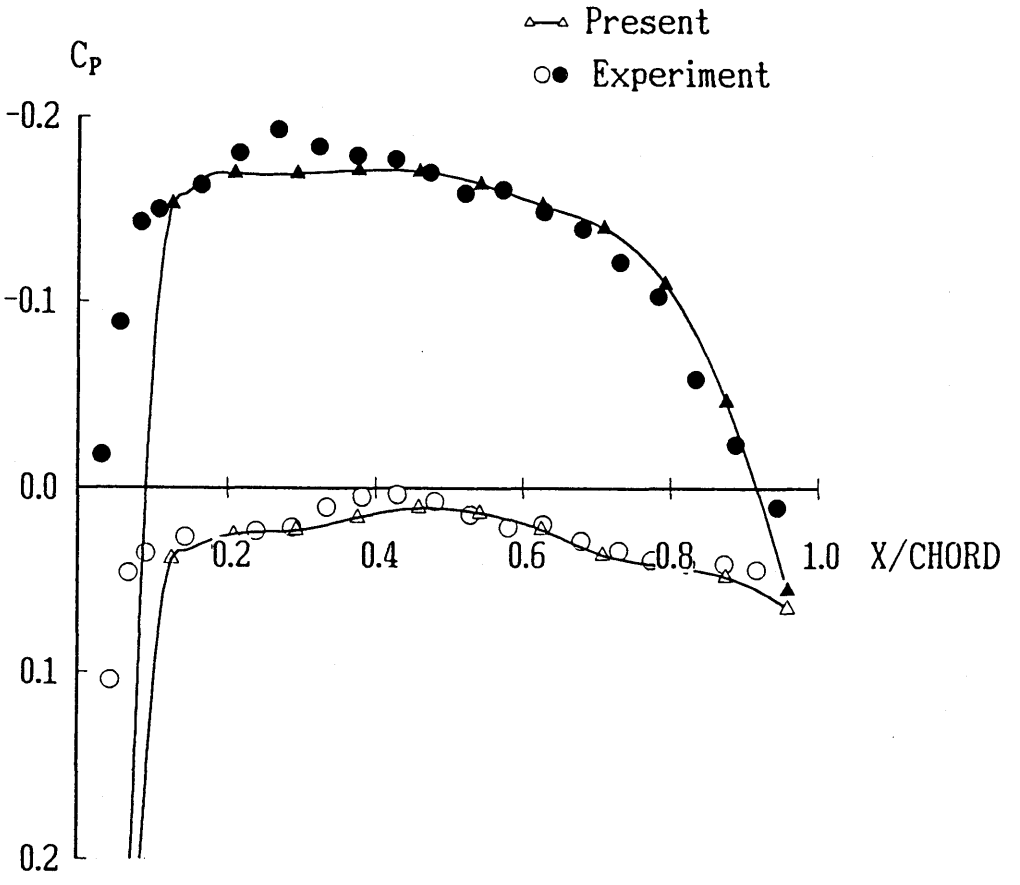


Fig. 5 Pressure distribution on DTRC4119
(Devised Wake, 0.7 Radius)

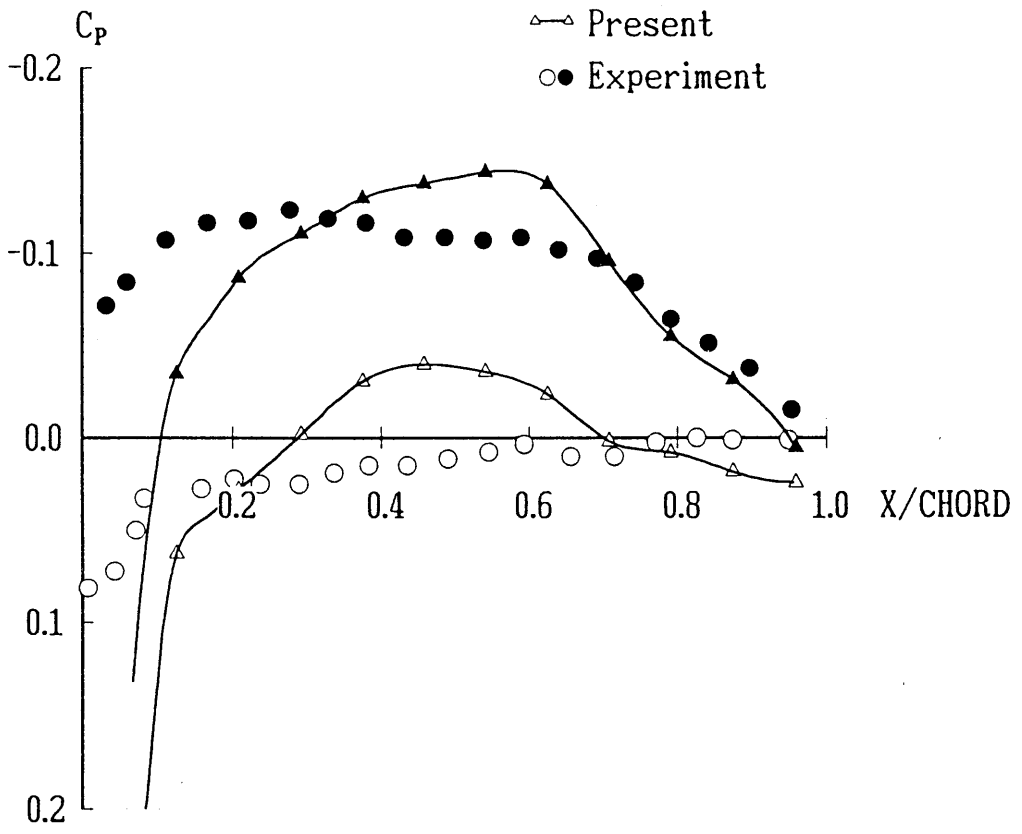


Fig. 6 Pressure distribution on DTRC4119
(Devised Wake, 0.9 Radius)

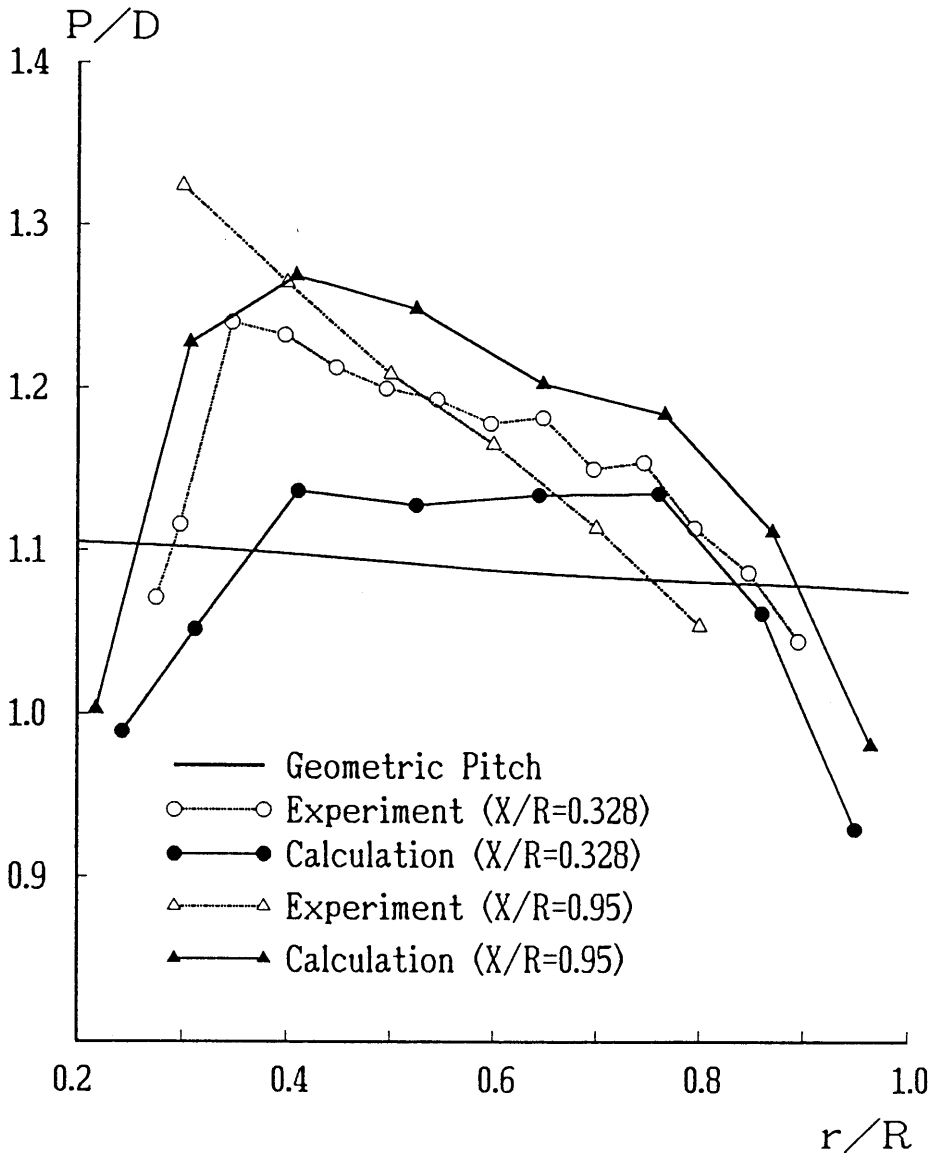


Fig. 7 Distribution of Blade Wake Pitch for DTRC4119

# APPENDIX F

## Calculations by CETENA

# Propanel: A Surface Panel Method for the Steady Analysis of Naval Propellers.

Giovanni Caprino[1] , Luca Sebastiani[1] , Mario Caponnetto[2] , Massimo De Benedetti[3]

[1]CE.TE.NA, Centro di studi di Tecnica Navale, Genova, Italy.
[2]CE.TE.NA Consultant, Genova, Italy.
[3]Physics Department, University of Genova, Italy.

## 1. Introduction

The present method, devoted to the steady analysis of naval screw propeller, is based on a low-order potential field formulation of the problem: constant distribution of sources and dipoles are placed on flat quadrilateral panels, so that the integral equation of the boundary value problem is transformed in an algebraic linear system. This system is solved numerically with the Gauss-Siedel method. At this step of development, no wake-relaxation is performed.

The Kutta condition is implemented by a linear interpolation between two values, one of which is that of Morino approximation [1]. The improvement of the results, compared with those of the Morino approximation, are quite satisfactory, maintaining on the other hand the same advantages in terms of calculation speed and implementation simplicity.

The calculation of the velocities is performed by numerical differentiation of the perturbation potential on the surface of the blades, through quadratic interpolation of the perturbation potential.

The results of the analysis for two test cases, a non-skewed three-bladed propeller and a highly-skewed five-bladed propeller, are given for the design condition.

For the first propeller we have chosen uniform radial and chordwise spacing, while for the second one a cosine spacing in the chordwise direction and a sine spacing for the radial direction have been selected [2].

## 2. Basic theory.

The computational procedure is based on a low-order lifting-potential panel method, which consists in discretizing the relevant boundaries with flat quadrilateral elements on which a constant singularities distribution is placed. The boundary value problem is solved numerically at the control point of each panel.

The calculation of the influence matrix is based on the standard formulas for the potential field due to a constant distribution of source and dipoles on a quadrilateral panel [3]. The lowest-order far-field approximation is used when the distance between two control points is greater than 0.2 times the diameter of the propeller. This way a considerable saving in the computational time is achieved without any significant loss in the solution accuracy.

The system of linear equations for the perturbation potential is solved using iterative Gauss-Siedel method.

The surface velocities are obtained by numerical differentiation of the perturbation potential. The direct numerical calculation has been preferred to the analytical approach, based on the velocity influence coefficients, because it is more efficient from the CPU-time

point of view, and it seems also to be more accurate [2].

As a results of the numerical procedure, the $C_p$ distribution on the blades and the torque and thrust coefficients are calculated.

The basic theory is inherently inviscid. Anyway a viscous correction to the inviscid thrust and torque coefficients is provided, taking into accounts the viscous effects on the blades surface on the basis of the two dimensional approach originally formulated by Van Oossanen [4].

A resistance coefficient Cr for each blade section is derived from the flat plank resistance coefficient Cf on the basis of the thickness-over-chord ratio t/c:

$$C_r = C_f\left(1+1.2\,t/c+70(t/c)^4\right)$$

The corresponding contribution in terms of thrust and torque is thence evaluated.

It should be stressed that this technique generally underestimates the viscous correction.

No wake relaxation is provided and a rigid helycoidal wake is adopted, with the pitch linearly varying from the corresponding value of the interested section to the mean value of the blade.

## 3. Panelling features.

For the non-skewed propeller, a coarser uniform spacing is used in the middle of the blade, while a finer uniform spacing is adopted near the tip, for the radial direction, and near the trailing and leading edges, for the chordwise direction.

Radial spacing is 0.05 r/R up to 0.9 r/R and 0.025 otherwise, chordwise spacing is 0.1 x/c from 0.1 x/c to 0.9 x/c and 0.025 otherwise.

The basic grid adopted for this propeller consists of 408 panels on each blade (see Fig. 1). An additional coarser grid with 260 panels has been analysed to assess the panelling sensitivity. The coarser grid has been obtained from the finer one using a larger radial spacing , namely 0.1 r/R , from 0.2 r/R to 0.9 r/R.

In the case of the highly-skewed propeller a cosine spacing for the chordwise direction:

$$x_c = \frac{1}{2}\left(1-\cos\left(\left(\frac{2\pi}{N}\right)(j-1)\right)\right) \quad j=1,\cdots,N/2+1$$

N = total number of the panels on the section

and a sine spacing:

$$x_r = \frac{R_h}{R}+\frac{R-R_h}{R}\sin\left(\frac{\pi}{2M}(m-1)\right) \quad m=1,\cdots,M+1$$

M(N/2+1) = total number of the panels on the blade

for the radial direction, have been considered to be more suitable to the complex blades geometry.

The basic grid adopted for this propeller consists of 728 panels for each blade (see Fig. 2).

The information on the blades geometry for both propellers has been derived from [5]. The features of blade stations and sections not reported in [5] are obtained by interpolation.

Hub is equally divided into Z portions, each further subdivided into six regions (see Fig. 3): the aft and forward ends, the intermediate region between trailing and leading edges, the portion at the intersection of the blade with the hub and two cylindrical portions between the ends and the intermediate region .

The panelling is helycoidal in the after part and cylindrical in the forward part. In the the intersection portion the grid consists of only one strip of panels, which match the corresponding panels on the blade.

The basic hub grid consists of 132 panels for the non-skewed propeller and

of 164 panels for the skewed one, for each blade portion.

## 4. Kutta condition.

The first step has been the implementation of the approximate Morino Kutta condition [1], imposing the equality of the strength of the dipole sheet on each strip of the vortex wake with the dipole jump on the corresponding panels adjacent to the trailing edge.

This way Kutta condition resulted generally not exactly satisfied at the trailing edge. On the hypothesis that the dipole sheet on the wake was underestimated, a correction of the original Morino condition was implemented consisting of a trial-and-error technique based on linear interpolation.

The technique starts with Morino approximation. Then Morino estimation for the dipole strength of the strips of the wake is multiplied by a guess coefficient, a value slightly larger than unity being sufficient. Finally the coefficient which makes the pressure jump at the trailing edge be zero, ensuring the satisfaction of Kutta condition, is found through linear interpolation between the two values.

Nevertheless its simplicity the method provided quite satisfactory (see Fig. 4).

## 5. Numerical procedures.

The features which mostly affect the results are the solution of the system of linear equations for the unknown dipoles distribution and the calculation of fluid velocities on the propeller surface.

The present linear equation solver is based on the Gauss-Siedel iterative method, which is felt to be more efficient than Gauss reduction especially for fine grid. The average iterations number needed for the solution of a linear system with 540 unknowns is 135.

Calculation of surface velocities distribution is performed by numerical differentiation of the potential on the basis of the panel control points on the propeller surface.

Differentiation is performed along two directions on the plane of the panel. To this purpose use is made of local non-orthogonal co-ordinates on the panel, which approximate the curvilinear abscissa on the propeller surface and are obtained joining each panel centroid with the mean point of the two adjacent panel sides. The projection on the local orthogonal co-ordinate system of the panel is performed at the initialisation stage during panelling procedure (see Figs. 5, 6).

fig. 5

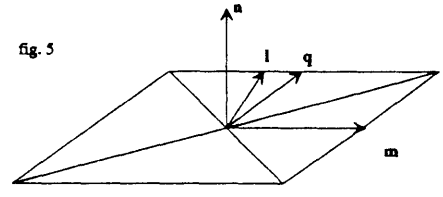


n, l, m, are the local orthogonal axes; q is the unit vector from centroid to mean point of the side

The differentiation algorithm consists in calculating the derivatives of the quadratic fit of the fluid potential through the adjacent panel control points expressed in terms of the curvilinear abscissa.

fig. 6

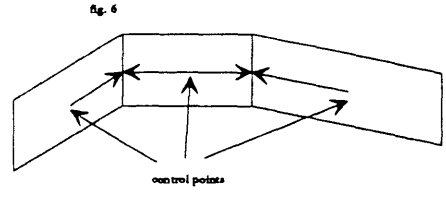


The quadratic fit of the potential is expressed by the parabola :

$$y^2 = as^2 + bs + c$$

The derivative along the directions m and q are thence found through the expression:

$$y'(s) = 2as + b$$

Choosing the origin of the curvilinear co-ordinates at the panel centroid, the derivative is simply equal to the coefficient $b$ of the parabola .

To give an idea of the computational speed of the complete procedure, the solution for the non-skewed propeller with the recomended panelling with 408 panels required one hour of CPU-time on a DEC Micro VAX 4000-200 for one calculation condition.

## 6. Results and discussion

The computational procedure has been applied to a three-bladed non-skewed propeller and a five-bladed skewed propeller.

The calculations have been performed at the design condition for both propellers, J = 0.833 and J = 0.905 respectively.

The viscous correction, described in paragraph 2, has been applied in the determination of the thrust and torque coefficients.

In the case of the non-skewed propeller the numerical results are compared with published data [5].

The results for the non-skewed propeller are illustrated in the figures from 7 to 10.

In Fig. 7 the $C_p$ distribution on the blade, obtained for the basic panelling with 408 panels, is presented at three r/R values (namely 0.3, 0.7 and 0.9) and compared with the experimental data. The agreement between numerical results and experimental data is generally good except at 0.3 r/R. The observed discrepancy is attributable to the blade-hub interference.

In Fig. 8 the corresponding results for the coarser grid with 260 panels are compared with the previous ones and the experimental data. It can be observed that there is no sensible difference between the two grids.

In Fig. 9 the results with and without hub are compared in terms of $C_p$ distribution on the blade to investigate hub influence. As expected the results are significatively different only for the section nearest to the hub, namely at r/R = 0.3.

In Fig. 10 $K_t$ and $K_q$ values are presented for J from 0.5 to 0.9, with and without viscous correction. It can be noted that the influence of viscous effects on Kt is quite small and the numerical results are in very good agreement with the experimental ones. The discrepancy between the calculated and measured $K_q$ is attributable to the presence of viscous effects, which are underestimated by the present correction technique.

In Fig. 11 the results for the case of the skewed propeller are presented in terms of Cp distribution on the blade at r/R = 0.4, 0.7 and 0.9 for the recommended panelling with 728 panels.

Nevertheless the satisfactory results of this preliminary correlation , further comparison of the numerical results with experimental data for other kinds of propellers is needed to completely validate the procedure and to assess its effectiveness from the propeller designer point of view. The present completion of the Cavitation Tunnel of Genova University seems to be a good basis for future work in this direction.

Finally it must be stressed that the present procedure is not the ultimate product of our research program but the first step towards the development of a complete panel method for propeller analysis.

## 7. Acknowledgement

The authors wish to thank the Department of Physics of Genova University for the co-operation in the theoretical and numerical formulation.

The appreciation of the authors is extended to the Institute of Naval Architecture of Genova University for the active interest in the development and application of the procedure.

## 8. List of references

[1] Morino, L. and Kuo, C.-C., "Subsonic Potential Aerodynamics for Complex Configurations: A General Theory," *AIAA Journal*, Vol. 12, No. 2, Feb. 1974.

[2] Kerwin E. J. et al., "A Surface Panel Method for the Hydrodynamic Analysis of Ducted Propellers," *SNAME Trans.*, Vol. 95, 1987.

[3] Hess, J. L., "The Problem of Three-Dimensional Lifting Flow and Its Solution by Means of Surface Singularity Distribution," *Computer Methods in Applied Mechanics and Engineering*, Vol. 4, Nov. 1974.

[4] Van Oossanen, P., "Calculation of Performance and Cavitation Characteristics of Propellers Including Effects of Non-uniform Flow and Viscosity", *NSMB* Publ. N. 457.

[5] Yessup, S. D., "An experimental Investigation of Viscous Aspects of Propeller Blade Flow," Ph.D. thesis, The Catholic University of America, 1989.

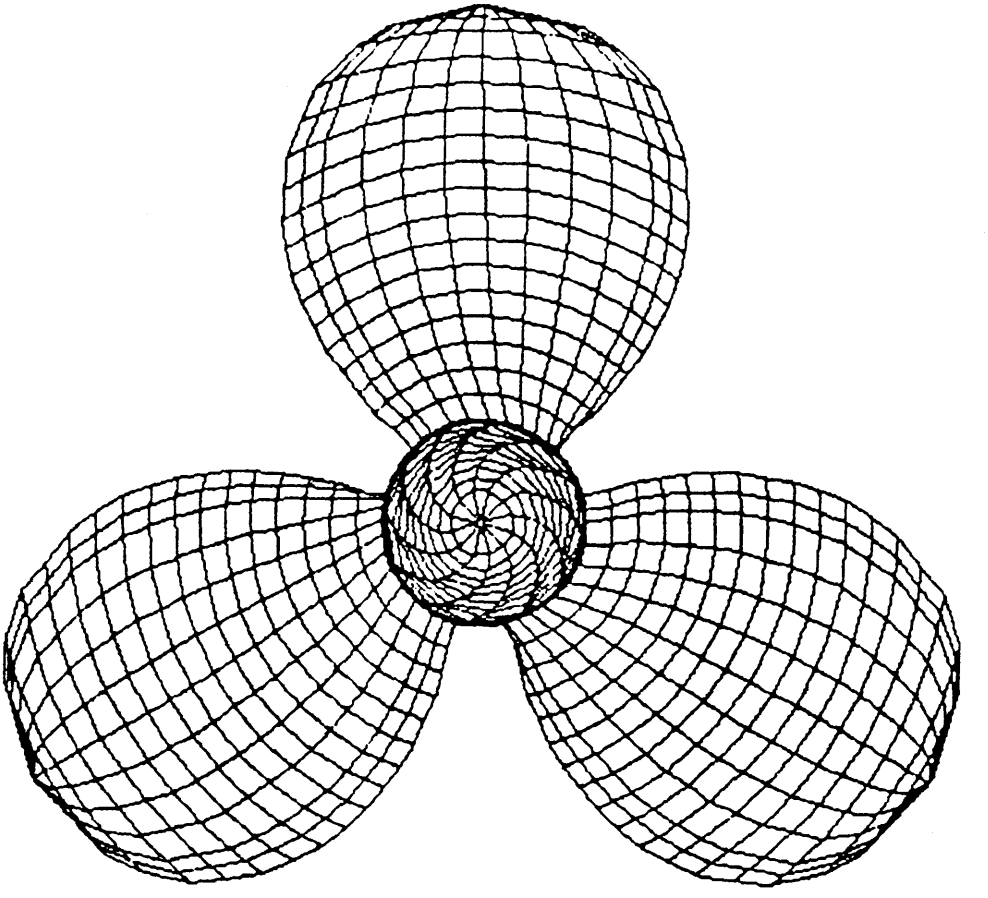

fig. 1. Basic grid for non-skewed propeller.

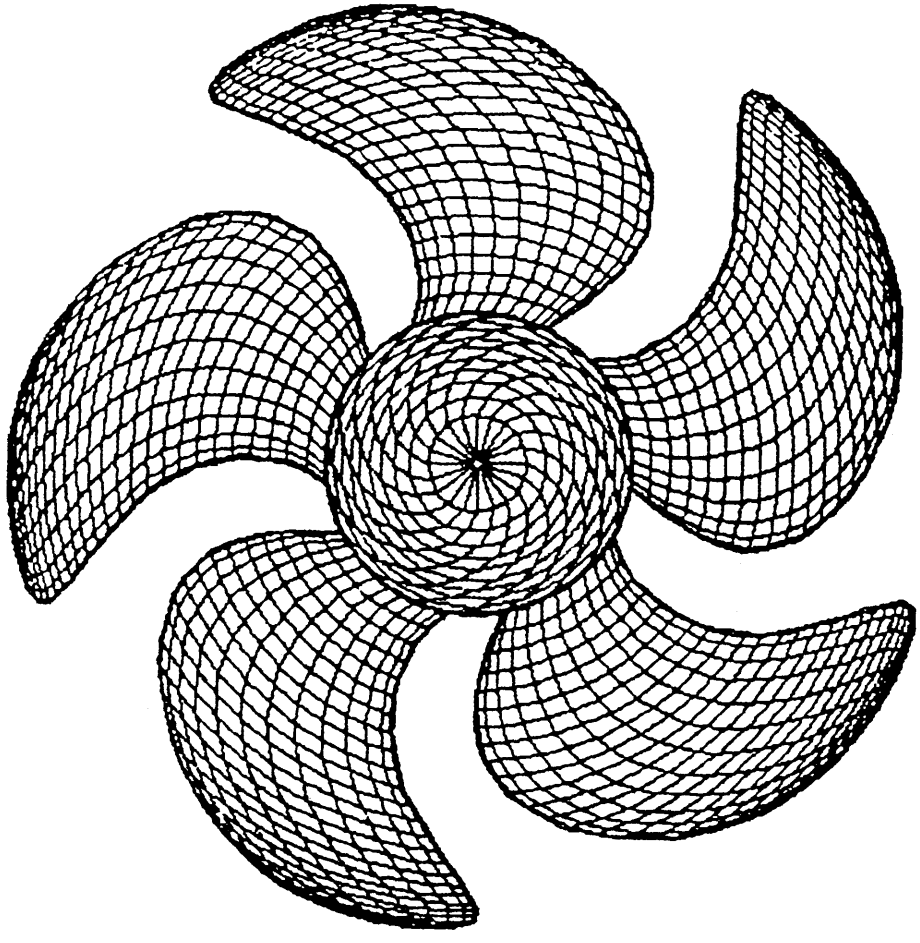

fig. 2 Basic grid for skewed propeller.

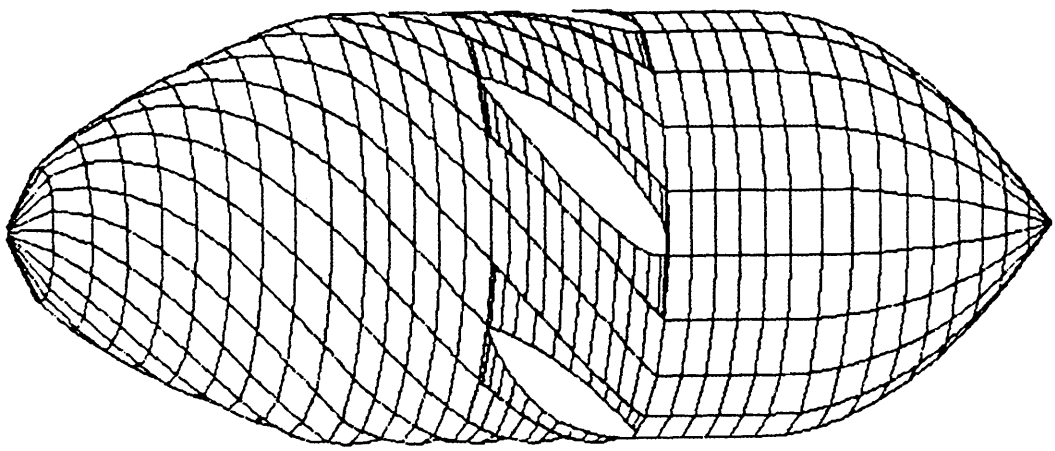

**fig. 3 Hub grid**

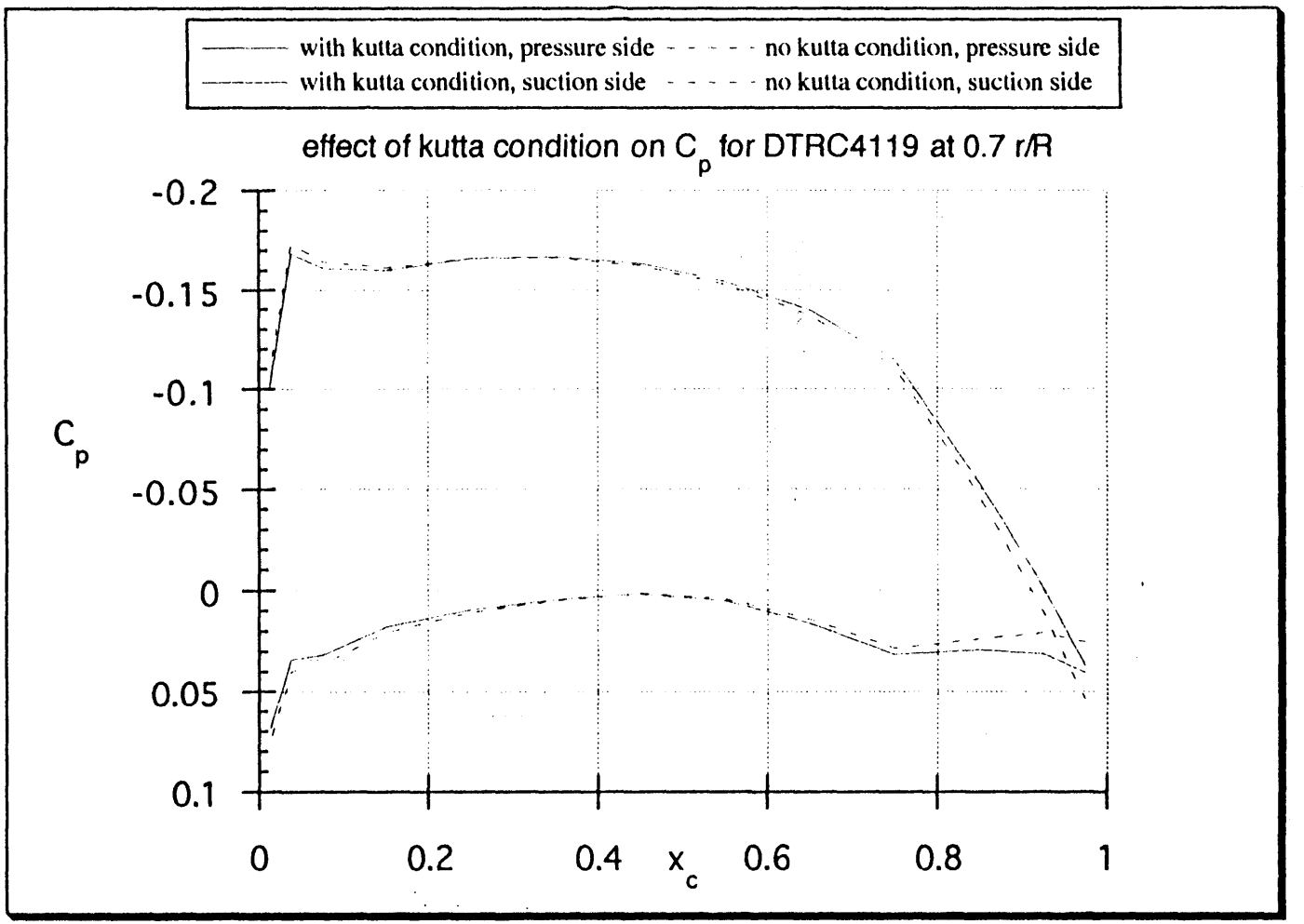
with kutta condition, pressure side
no kutta condition, pressure side
with kutta condition, suction side
no kutta condition, suction side
effect of kutta condition on $C_p$ for DTRC4119 at 0.7 r/R
$C_p$
-0.2
-0.15
-0.1
-0.05
0
0.05
0.1
0
0.2
0.4
$x_c$
0.6
0.8
1

fig.4

$C_p$ distributions for propeller DTRC4119 at various values of r/R for J=0.833

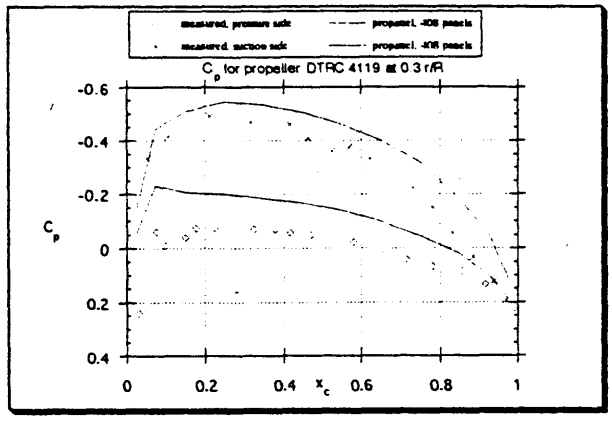


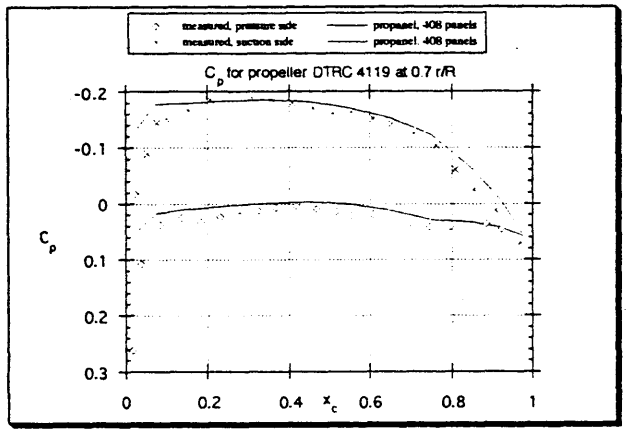


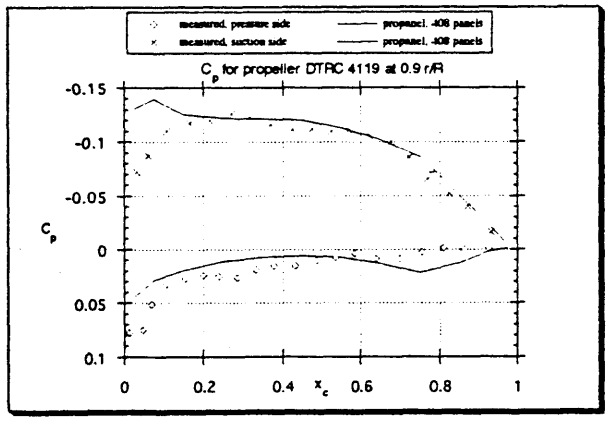


fig.7

$C_p$ distributions for propeller DTRC4119 at various values of r/R for J=0.833

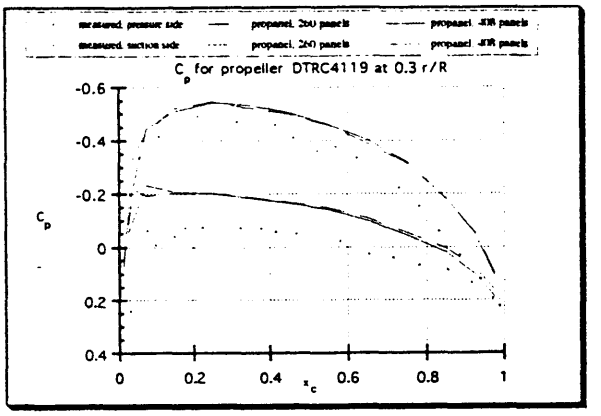


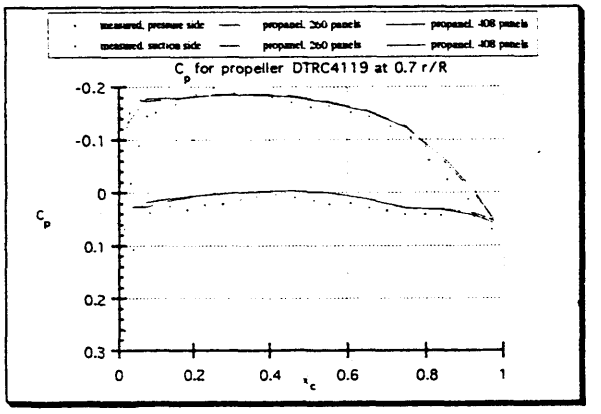


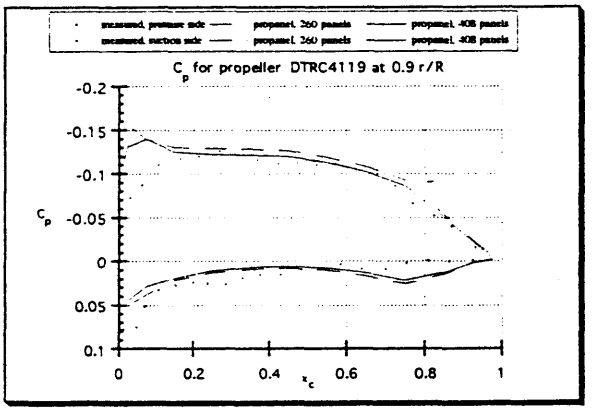


fig.8

$C_p$ distributions for propeller DTRC4119 at various values of r/R for J=0.833 with and without hub

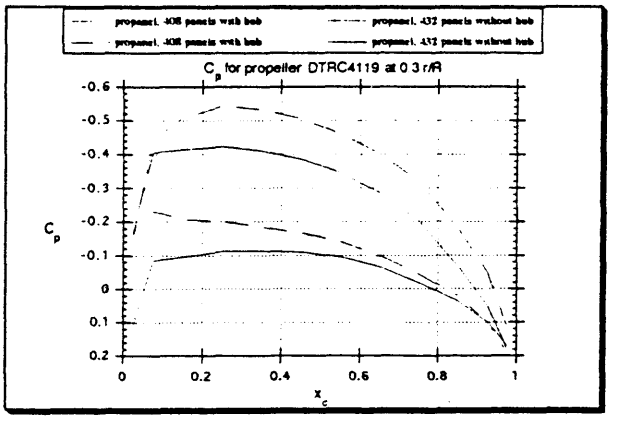


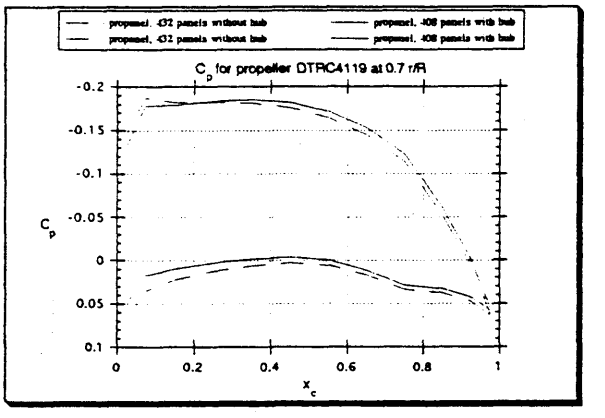


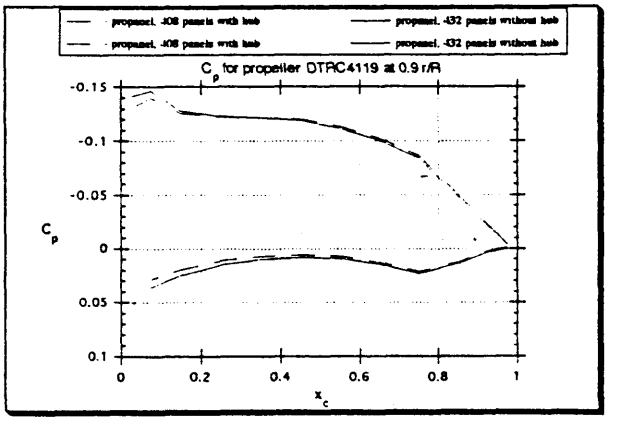


fig.9

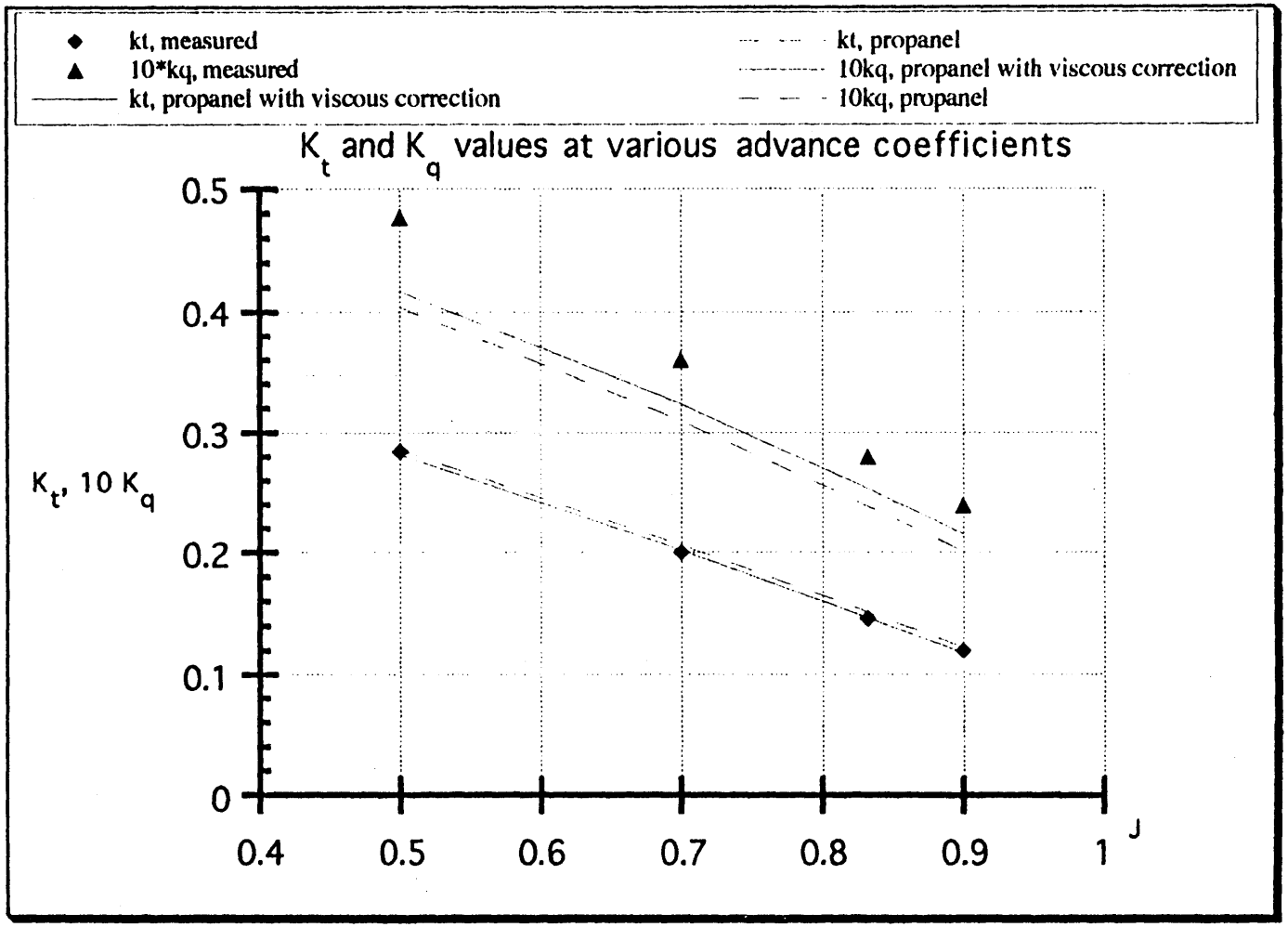
kt, measured
10*kq, measured
kt, propanel with viscous correction
kt, propanel
10kq, propanel with viscous correction
10kq, propanel
K_t and K_q values at various advance coefficients
K_t, 10 K_q
0.5
0.4
0.3
0.2
0.1
0
0.4
0.5
0.6
0.7
0.8
0.9
1
J

fig.10

$C_p$ distributions for propeller DTRC4842 at various values of r/R for J=0.905

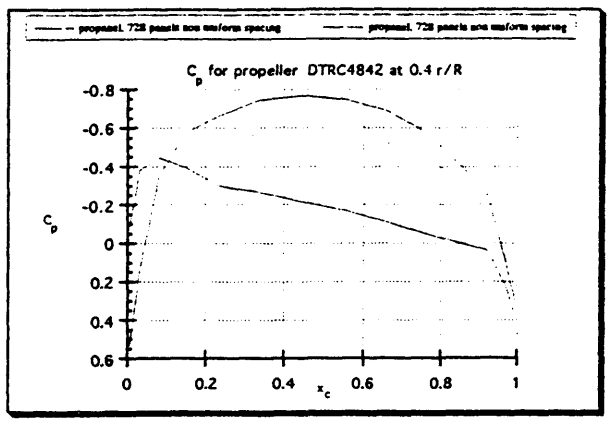


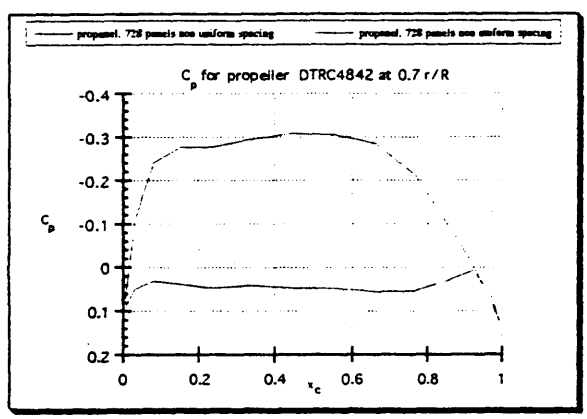


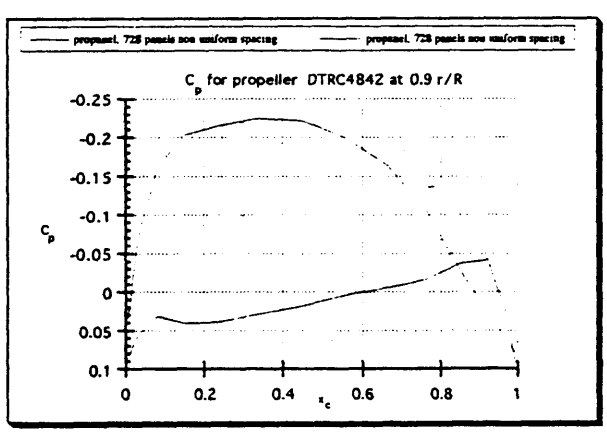


fig.11